Meccanica
https://doi.org/10.1007/s11012-024-01885-0

RESEARCH

Comparative analysis between continuous and discontinuous methods for the assessment of a cultural heritage structure

Mattia Schiavoni · Francesca Roscini · Francesco Clementi

Received: 14 July 2024 / Accepted: 14 September 2024

Abstract In an era marked by the urgent need to ensure the safety of existing buildings according to current standards, evaluating the stability of masonry structures against hazard events has become a significant challenge. Despite the versatility and durability of masonry, structural assessments are hampered by factors such as limited information on material properties, irregular geometries, and ageing. To address this issue, numerous modelling techniques have been developed, supported by extensive scientific literature. However, significant factors related to the case study replication, such as the geometric complexity, the mechanical behaviour of masonry, the loading applications, contribute to the challenges associated with modelling procedures, including computational time, discretization procedures, and step incrementation. This paper critically discusses the most innovative modelling approaches. Specifically, it aims to compare the efficiency of the Distinct Element (discontinuous) Methods and the Finite Element (continuous) Method, both applied to the numerical simulation of a case study structure severely damaged by the 2016 Central Italy earthquake under lateral loading conditions. The continuous method is analysed using Midas FEA NX©, while the discontinuous methods are studied using 3DEC© and LMGC90© software, each with different contact conditions. Finally, the investigation highlights the main advantages and disadvantages of each method. In particular, the discontinuous method demonstrates reliability in accurately replicating failure patterns, whereas the continuous method allows for a faster model setup, making it suitable for preliminary studies on structural dynamics.

Keywords Continuous method · Discrete element method · Masonry · Collapse mechanisms · Non-linear dynamic analysis

1 Introduction

Over the centuries, historical masonry constructions have shown their susceptibility to dynamic loads, mainly earthquakes. Recent seismic events in central Italy between 2016 and 2017 have highlighted the fragility of these structures [1–5]. Irregular geometry, varying historical development, inadequate maintenance, and the lack of effective structural behaviour, such as box-like action, have been identified as the primary factors contributing to their vulnerability [6–8].

M. Schiavoni · F. Clementi (✉)
Department of Construction, Civil Engineering and Architecture (DICEA), Università Politecnica delle Marche, Via Brecce Bianche 12, 60131 Ancona, Italy
e-mail: francesco.clementi@univpm.it

F. Roscini
Department of Engineering, Niccolò Cusano University, Via Don Carlo Gnocchi 3, 00166 Rome, Italy

Published online: 08 October 2024

The conservation and restoration of historical buildings, specifically those to be considered as part of the cultural heritage, are becoming increasingly important in Europe, while preserving their main architectural features. This is especially true in Italy, where the world's largest percentage of monumental churches, monasteries, and towers is located. The earthquakes recorded in the recent decades (Umbria-Marche 1997–1998, Abruzzo 2009, Emilia-Romagna 2012, Marche-Lazio-Umbria-Abruzzo 2016–2017) have severely damaged numerous unique architectural heritage structures [9–11].

Ensuring the protection of Europe's and Italy's rich architectural heritage necessitates a thorough assessment of historical constructions' vulnerability to earthquakes [12]. Unlike modern structures, most historical buildings are constructed from masonry, which is not inherently designed to withstand lateral forces. Traditional design methods prioritized gravity loads, neglecting aspects like lateral resistance and ductility [13]. Further complicating matters, many historical buildings now serve various purposes, including residences, offices, museums, and critical civil service facilities. Buildings designated for strategic roles during disasters, such as housing rescue team headquarters or providing temporary shelter to displaced persons, require even greater safety considerations [14, 15]. Consequently, these structures must be able to withstand both vertical and horizontal loads effectively.

Historical masonry structures present unique challenges for seismic analysis due to their inherent complexity and limited understanding of their structural behaviour, particularly under earthquake loads. Compared to modern buildings, these structures are typically more massive and primarily designed to resist compressive forces. The successful development of reliable mathematical models is crucial for the seismic assessment and retrofitting of such structures. For modern buildings utilizing well-defined industrial materials like reinforced concrete and steel, the consistent properties of materials and structural elements enable the development of reliable models [16, 17]. However, accurately evaluating the seismic response of historical masonry structures is significantly more complex. This complexity arises from several factors, including the variability in material properties, geometric irregularities, variations in floor stiffness (influencing diaphragm action), and the often-intricate connections between orthogonal walls and both structural and non-structural elements [6, 18–21].

In conventional engineering practice, assessing masonry structures often relies on an equivalent frame approach [22]. This method, derived from post-earthquake damage observation, models vertical masonry elements as piers and sections between openings as spandrels, assuming both to be prone to cracking or failure and connected by rigid nodes. However, these assumptions are not suitable for historical buildings due to their complex and evolving construction histories [23].

Since the 1990s, advancements in scientific research have yielded more sophisticated modelling techniques specifically tailored for heritage masonry structures [24–27]. Two prominent methods, block-based (discontinuous) and continuous (homogenization) models, offer more accurate numerical responses compared to real-world damage scenarios [28, 29]. The block-based (discontinuous) approach captures the distinct behaviour of individual blocks and mortar in the masonry response. This method encompasses detailed micro-modelling, where both blocks and mortar are explicitly represented [30, 31] as well as simplified versions where mortar thickness is incorporated into block dimensions [32, 33]. These approaches can be implemented using either Finite Element (FE) or Discrete Element (DE) methods.

In the FE approach, masonry is discretized into regular elements that interact through interfaces governed by frictional or cohesive laws [34]. These parameters are calibrated based on experimental testing. The DE method, on the other hand, represents masonry as individual blocks interacting through contact surfaces, often using non-smooth or smooth contact laws. The key strength of the block-based (discontinuous) approach lies in its ability to simulate block separation and potential crumbling of multi-leaf masonry walls. This allows for a unified analysis of both in-plane and out-of-plane structural behaviour [35–40].

Conversely, the continuous method assumes perfect connectivity between all masonry elements, enabling a detailed description of the in-plane structural response. Material heterogeneity is treated as a continuous deformable body governed by appropriate constitutive laws for static and dynamic loads [13, 41–44]. These laws can be derived from experimental

tests [45], similar masonry properties, or national/international regulations. Compared to the block-based approach, the continuous method offers faster model creation and analysis execution [43, 46, 47].

This paper explores the contrasting strengths of the block-based (discontinuous) approach using the DE method and the continuous method using classical FE with solid elements. Both approaches are applied to a significant case study: the church of S. Nicolò in Sentino (Fig. 1), located in a hamlet of Camerino within the Macerata Province of central Italy. The village experienced extensive damage during the earthquake of August 24th, 2016, making this church one of the oldest remaining structures in the area.

Finally, this investigation highlights the main advantages and disadvantages of each method. The discontinuous method excels in accurately replicating failure patterns, while the continuous method offers faster model setup, making it suitable for initial studies on structural dynamics.

2 Historical developments and the seismic damage of 2016

This study examines the Church of San Nicolò in Sentino, Italy, a historical masonry structure that serves as a case study for the application of seismic analysis methods. The church, located on the outskirts of Sentino's inhabited center, is a stone-built building with exposed masonry (Fig. 1). Its Romanesque origins date back to the thirteenth century, as documented in the Rationes Decimarum.

The Church of San Nicolò in Sentino represents the collaborative efforts of individuals and the community. It embodies the characteristics of isolated, rural, rectangular churches typical of the Romanesque period. The design prioritizes simplicity, reflecting the fundamental principle of 'economy' prevalent in historical construction practices. Local materials and craftsmanship were employed, resulting in a structure devoid of complex features like cross vaults, domes, loggias, or multiple naves. Conversely, the church features small single windows, a truss roof, a few 'oculi' (circular windows), and arches. Both geometrically and materially, the church presents a straightforward construction, built entirely from locally sandstone.

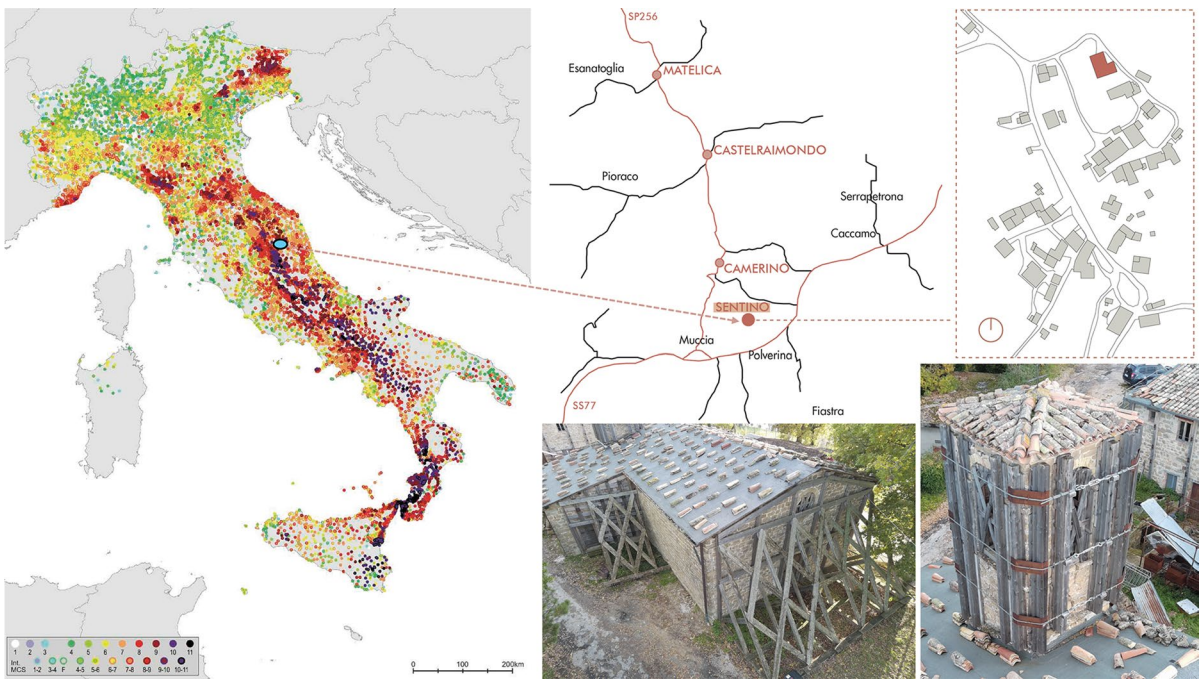

Fig. 1 Sentino, hamlet of Camerino, central Italy

Although its apparent simplicity and modesty, the church exhibits a refined elegance and attention to detail. The main façade features a rose window, while the rear façade includes a single window. Internally, the camorcanna vaults (vaults with intersecting ribs), a coffered ceiling adorned with intricate carved roses, and a collection of ancient and valuable frescoes all contribute to the church's historical significance and preservation value. The layout of this former parish church follows a rectangular plan (dimensions: 15.60 m × 9.50 m) designated for religious functions. A superimposed bell tower and a smaller, more compact structure adjoining the main building served as the sacristy.

The church has experienced numerous seismic events throughout history within the pre-Apennine Camerte region; from the past and destructive earthquakes of 1741 and 1799 to the more recent ones of 1997 and 2016, that provided serious damage to the structure, compromising its overall stability (Fig. 2). The historical analysis of this cultural heritage allows to understand the interaction between building blocks constructed in different eras. This complex issue is depending on the masonry quality, its heterogeneity, and the degree of connection between the different structures. In general, more recent structural modifications are not connected to the pre-existing ones, creating potential stability and safety issues.

The structural transformation began in the nineteenth century with the subsequent enlargements of the sacristy and the bell tower, positioned 5 cm from

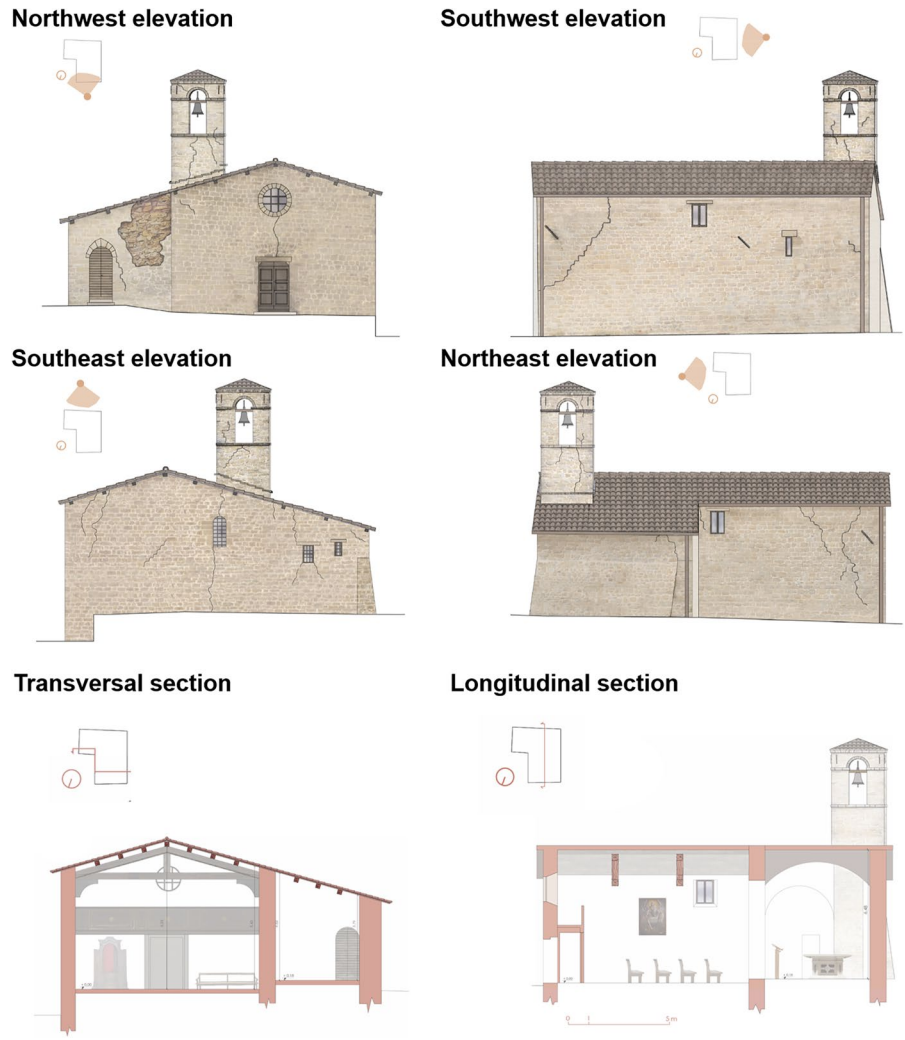

Fig. 2 The four façades with the damage after the seismic sequence of 2016, the transversal and longitudinal sections

Fig. 3 Detail of the damage inside the church and of the windows near the bell tower placed at 5 cm from the back wall

the frescoed back wall (Fig. 3), covering a portion of it and hiding the existing 'monofora' window.

Subsequently, to balance the architectural symmetry, an accessory room was built mirroring the bell tower, covering the frescoed 15th-century apse. The entire presbyterial area was then enriched and covered with barrel vaults and camorcanna. In 1928 the church underwent a restoration intervention, and a wooden false ceiling was built in the church hall and a choir loft, also in wooden structure, supported by small pillars.

After the 1997 earthquake, the load-bearing perimeter walls exhibited various cracks and serious fractures, mainly in the lower part of the structure. More critically, the upper masonry was detached, with no connection to the wooden beams. The external walls were characterized by de-cohesion of the masonry with several stones expelled due to the degradation of the mortar beds. Also, the foundations exhibited significant settlement, especially in the rear presbytery area and the lateral part of the small church. In addition, the foundations were in poor condition due to moisture infiltration, which had damaged and degraded the mortar.

In 1999, rehabilitation works aimed at both restoring the damaged elements and improving the overall structural load-carrying capacity by seismic retrofitting interventions. In particular, the reinforcement process involved: firstly, the masonry walls were strengthened by cracks repairing, and thus their connections between orthogonal elements were improved to prevent overturning mechanism. Moreover, a complete overhaul of the roof was planned, with a non-thrusting covering. Then the foundations were consolidated, and the presbytery area was restored. The interventions in 1997 improved the monolithic behaviour of some masonry walling. In 2002, a significant modification was made. Nevertheless, seismic sequences occurred in 2016 had revealed major structural weaknesses and inadequacies in the interventions performed a few years prior. Masonry disintegration occurred again in other areas of the structural aggregate. Despite the interventions after the 1997 earthquake, the external walls exhibited

out-of-plane failure mechanisms due to the degradation of the mortar beds and the lack of connection between the wooden beams and the masonry (Fig. 2). The northeast façade of the sacristy experienced disintegration and partial expulsion of the external wall. This disintegrative behaviour can be attributed to the poor quality of the mortar and the insufficient number of diatoni within the structure to ensure rigid body behaviour. In addition, multi-leaf masonry walls result critical owing to the pressure of the infill to the external walls. The northwest façade, the church's main front, shows failures along the mortar joints, because of the poor mechanical quality. A passing crack along the mortar joints near the southwest façade of the church indicates an attempt to drag part of the counteracting wall. Two oblique cracks in the northeast counteracting wall also confirm the mechanism's activation. The southwest façade of the building shows cracks primarily in the upper part and along the mortar joints, with a significant pseudo-vertical crack above the 'monofora' window, indicating an attempt to expel the sandstone blocks. Significant damage was also observed in the bell tower, where the masonry is severely cracked and almost disintegrated in several places (Fig. 2).

In summary, the vulnerability of the wall to horizontal forces could be influenced by several reasons: the absence of top restraints, ineffective connections with orthogonal walls, and a lack of bond beams or ties. These factors can provide the activation of a composite overturning mechanism, highlighted by a diagonal crack in the orthogonal walls of the nave. This mechanism involves the rigid rotation of the wall around a horizontal hinge, dragging portions of the masonry from the counteracting walls. A fast-securing system on this façade was installed in 2018 in guaranteeing its integrity.

Therefore, measures were taken to secure the religious building by implementing interventions to maintain the unity of the masonry structure in the most damaged parts.

3 Numerical models

This study presents a comparative analysis of two distinct modelling approaches for evaluating the Church of San Nicolò's dynamic behaviour under seismic loads: the Discontinuous Model (DM) and the Continuous Model (CM). The most significant distinction between these methodologies resides in their respective approaches to material nonlinearities.

The DM assumes that material nonlinearities are primarily concentrated within the mortar joints, representing the church structure as an assembly of individual blocks. Whereas the CM simplifies the structure by assuming material homogeneity, distributing nonlinearities uniformly throughout the entire volume of solid elements.

Each approach employs distinct computational algorithms. For the DM analysis, the Discrete Element Method (DEM) and the Non-Smooth Contact Dynamics (NSCD) are implemented respectively in 3DEC© [48] and within LMGC90© software [49, 50]. These methods account for the discrete shape of the masonry blocks and their interaction at mortar interfaces.

On the other hand, the CM has developed in Midas FEA NX© [51] based on the Concrete Damage Plasticity (CDP) model. In this approach, the masonry is considered as a continuum, simplifying the analysis but potentially neglecting the influence of mortar joint behaviour on the overall response.

The mechanical parameters have been calibrated according to the Italian regulations of 2018 [52], as outlined in Chapter 8, and the corresponding explanatory circular of 2019 [53]. The mechanical parameters considered are listed in Table C8.5.I of [53] for the type of masonry referred to as "Random Rubble Masonry" (hereafter referred to as bad masonry) and "Solid Bricks and Lime Mortar" (hereafter referred to as good masonry). The tensile strength has been assessed as equal to one-tenth of the compressive strength. The parameters have been reduced by a confidence factor of 1.35 [52].

The following section provides a brief overview of the DEM, NSCD, and CDP methods. Theoretical details can be found in-depth in the referenced sources [48, 54–56].

3.1 Discontinuous models

The DM approach employed two software packages: 3DEC© [48] and LMGC90© [49, 57]. In this method, the structure was discretized into an assembly of distinct blocks, resembling a simplified micro-modelling approach. The block dimensions incorporated the mortar thickness. The nonlinear behaviour of the

masonry, arising from interactions between blocks, was addressed using Discrete Element Methods (DEM) in 3DEC© and Non-Smooth Contact Dynamics (NSCD) in LMGC90©. To facilitate a direct comparison between the two discontinuous approaches in this study, rigid blocks within the DEM framework are used.

3.1.1 Geometry

The geometry of the church and the configuration of its constituent blocks present a considerable technical challenge for the automated generation of models using scripting or computer-aided design (CAD) software. In order to ensure the accurate depiction of each block's position, scaled images of the church were imported into AutoCAD©. The pictures were instrumental in the generation of a two-dimensional representation of the structure's façades, delineated by a series of lines. Subsequently, the 2D outlines were extruded to generate the 3D geometric model of the church's principal structure, as illustrated in Fig. 4.

The transfer of the church's geometry into LMGC90© using CAD files is a relatively straightforward process. However, this is not the case with 3DEC©. Although 3DEC© has the capability to import and export CAD files in DXF and STL formats for 3D surfaces, it also allows for the modification of polyhedrons (the 3D representations of objects in 3DEC) via DXF files. Nevertheless, a limitation of the integrated import command (polyhedron cube) is its restriction to creating boundaries in two dimensions. Consequently, an alternative approach is necessary to generate complex three-dimensional geometries.

The method employed here involved developing a script that converts the 3D geometry into a format compatible with 3DEC©. Specifically, the script produces a text file that utilizes the polyhedron prism command to represent blocks within 3DEC©.

3.1.2 Discrete element method (DEM) in 3DEC©

The present work utilizes the Discrete Element Method (DEM) implemented in 3DEC© [48]. This method represents the structure as an assembly of rigid or deformable blocks interacting through contact points (Fig. 5). Unlike the Non-Smooth Contact Dynamics (NSCD) method, DEM employs an explicit integration scheme for numerical stability,

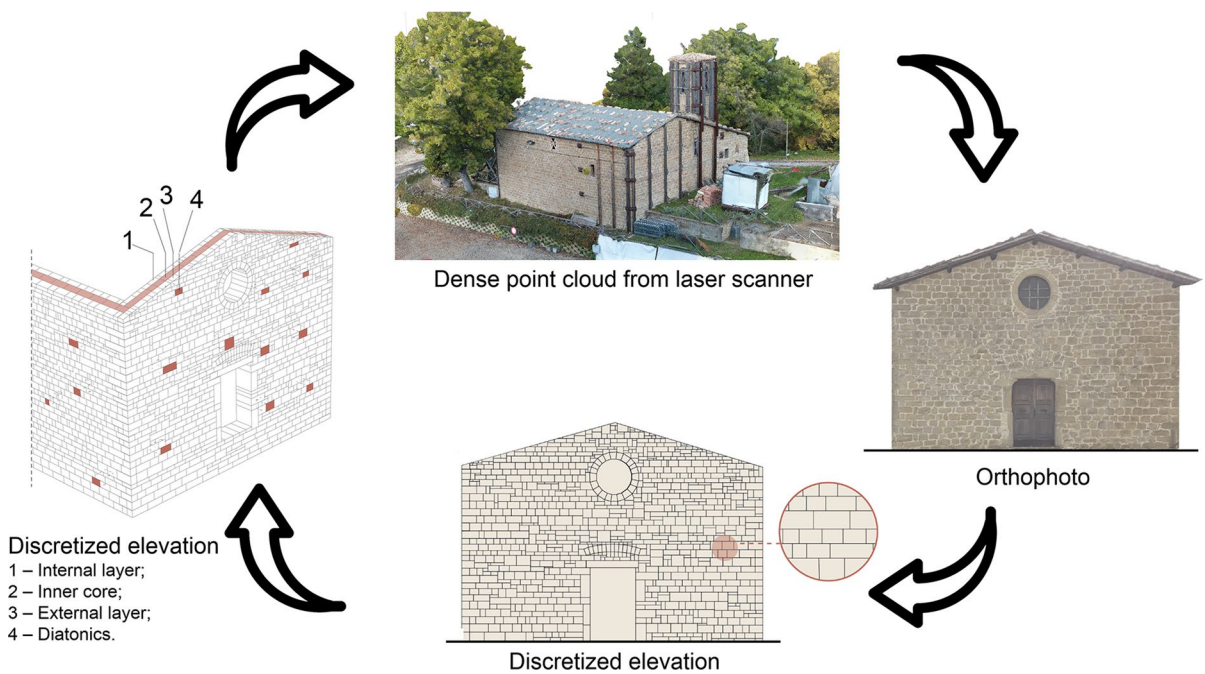

Fig. 4 Steps for creating the texture of the DEM

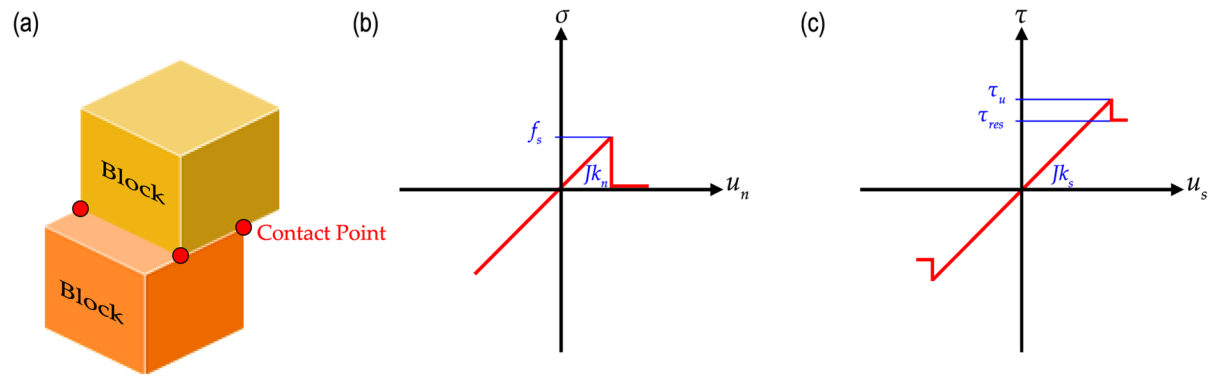

Fig. 5 Mechanical representation of the contact point between blocks (**a**), laws in the normal direction (**b**), and the shear direction (**c**)

often incorporating damping, employing the central difference method.

The interaction between blocks is governed by linear or non-linear contact laws in both the normal and shear directions. Each block and its associated joints are further discretized into internal particles (Fig. 5.a). These particles interact with neighbouring blocks through contact points. Contact laws (Fig. 5b, c) define the relative movement at these interfaces. The parameters of the joints used in 3DEC are provided in Table 1. A pair of springs at each contact point facilitates the transfer of normal (Eq. (1)) and shear forces (Eq. (2)) between blocks:

$$\Delta\sigma_n = Jk_n \Delta u_n, \tag{1}$$

$$\Delta\tau_s = Jk_s \Delta u_s. \tag{2}$$

Within the DEM framework, the state of failure corresponds to a nullification of both the cohesion (c) and the normal stress σ_n; however, the friction angle (ϕ) remains unaffected. Sliding between blocks is initiated when the shear force (τ) reaches a critical value, defined as:

$$|\tau_s| = c + \sigma_n tan\phi = \tau_{crit} \tag{3}$$

Here, σ_n represents the normal stress acting across the contact surface. This equation reflects the influence of both cohesion (c) and friction angle (ϕ) on the shear resistance, with σ_n playing a role by amplifying the frictional resistance through the tangent term.

If the normal tension (σ_n) exceeds the tensile strength (f_t):

$$\sigma_n = 0. \tag{4}$$

In the proposed model utilizing an explicit time-stepping algorithm, the equations of motion for each node of the rigid blocks are as follows:

$$m\frac{d\dot{u}_i}{dt} + \alpha m\dot{u}_i = \sum f_i, \tag{5}$$

where u_i is the nodal displacement vector of a node ($i = \{x, y\}$), m is the nodal mass, α is the mass-proportional viscous damping constant. The total nodal force vector $\sum f_i$ is given by a sum of three terms:

$$\sum f_i = f_i^C + f_i^E + f_i^A, \tag{6}$$

Table 1 Joints' parameters used in 3DEC©

	JKn (Pa/m)	JKs (Pa/m)	Jfric (°)	Jcoh (Pa)	Jten (Pa)	W [kN/m^3]
Church	1.13E+10	4.53E+09	27	1.00E+05	5.00E+04	20
Inner rubble	2.67E+10	1.07E+10	17	1.00E+05	1.00E+05	19
Tower	1.33E+10	5.33E+09	27	1.00E+05	1.00E+05	18
Foundation	7.67E+09	3.07E+09	42	1.00E+05	1.00E+05	20

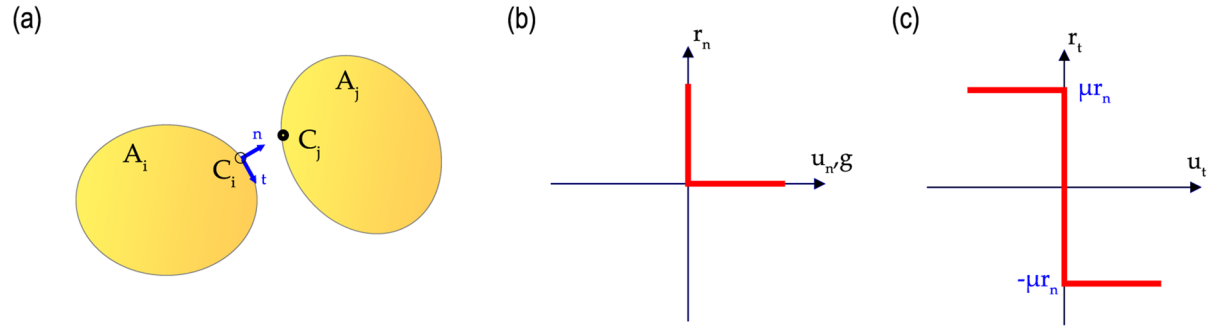

Fig. 6 Contact between bodies (**a**), Signorini's law (**b**) Eq. (6), and dry-friction Coulomb's law (**c**) Eq. (8), where **M** is the mass matrix, $\ddot{\boldsymbol{q}}$ is the acceleration vector, $\boldsymbol{f}(q, \dot{q}, t)$ represent the internal and external discretized forces acting on the system, respectively, and $\boldsymbol{l}$ is the resultant of contact

where f_i^C represents the contact forces, f_i^E is the nodal forces from the internal stresses and f_i^A is the sum of the external applied loads, including gravity.

3.1.3 *Non-smooth contact dynamics (NSCD) in LMGC90©*

The NSCD method [58, 59] utilizes an implicit integration scheme to incorporate non-smooth contact laws (Fig. 6). This approach involves considering two interacting bodies: the A_i candidate and the A_j antagonist. Potential contact points, denoted as C_j and C_i, are identified on these bodies, with n representing the unit vector normal to the contact point (Fig. 6a). The distance between these points defines the gap function (g):

$$g = (C_j - C_i)\boldsymbol{n} \tag{7}$$

Two contact laws are employed to determine the normal ($\dot{u}_n$) and tangential ($\dot{u}_t$) forces at the contact interface. These laws consider the relative velocity of the (C_j) with respect to the C_i along the normal (r_n) and tangential (r_t) directions, respectively. The resulting contact forces (**R**) employed by the A_j antagonist on the A_i candidate.

Signorini's Law of Impenetrability (Fig. 6b), Eqs. (8) and (9) define a perfect plastic impact, implying a zero coefficient of restitution according to Newton's Law. Therefore, this translates to negligible bouncing behaviour, relevant for materials like stones and bricks with low restitution coefficients.

$$g \geq 0, r_n \geq 0, g r_n = 0, \tag{8}$$

$$\text{if } g = 0 \rightarrow \dot{u}_n \geq 0 \rightarrow r_n \geq 0 \rightarrow \dot{u}_n r_n = 0. \tag{9}$$

Equation (10) represents the dry-friction Coulomb's Law (Fig. 5c):

$$|r_t| \leq \mu r_n : \begin{cases} |r_t| < \mu r_n \rightarrow \dot{u}_t = 0, \\ |r_t| = \mu r_n \rightarrow \dot{u}_t = -\lambda \frac{r_t}{|r_t|}, \end{cases} \tag{10}$$

where μ is the friction coefficient and λ is a positive real arbitrary number.

The equation of motion for the system can be expressed as:

$$\boldsymbol{M}\ddot{\boldsymbol{q}} = \boldsymbol{f}(q, \dot{q}, t) + \boldsymbol{l}. \tag{11}$$

The couples associated with each contact, denoted as $(\dot{u}_n, \dot{u}_t)$ and (r_n, r_t), are governed by linear maps that depend on $\boldsymbol{q}$ the global vectors $\dot{\boldsymbol{q}}$ and $\boldsymbol{l}$, respectively.

Since Eqs. (8) and (9) are non-smooth, the contact forces (l) and velocities ($\dot{q}$) become discontinuous functions of time. While the velocities are discontinuous, Eq. (11) can be integrated over a time step (t). The equation of motion is then integrated over time intervals $[t_i, t_{i+1}]$ using the following approach:

$$\boldsymbol{M}(\dot{q}_{i+1} - \dot{q}_i) = \int_{t_i}^{t_{i+1}} \boldsymbol{f}(q, \dot{q}, t)dt + \bar{l}_{i+1} \tag{12}$$

Here, $\bar{l}_{i+1}$ represents the pulse at the time interval and $\dot{q}_{i+1}$ is the variable that approximates the right limit of the velocity at time $[t_{i+1}]$. The contact forces are approximated by averaging the pulse in $[t_i, t_{i+1}]$ within the global time step (Eq. 12) and the local

contact law constraints (Eqs. 8 and 9). By neglecting block deformability, the NSCD method captures the dynamic interaction between elements through sliding and oscillation of rigid blocks. The different numerical models are reported in Fig. 6. A friction coefficient equal to $\mu = 0.50$ was used at the interface between the blocks, equal to $\mu = 0.90$ in the interface between the blocks and the base, equal to $\mu = 0.30$ the external masonry and the filling.

3.2 Continuous model (CM)

The CM approach is implemented in a commercial software, Midas FEA NX© [51]. In this method, the masonry was simplified as a homogeneous isotropic material. Its nonlinear behaviour was governed by the Concrete Damage Plasticity Model (CDP) [56], which is a valid option for materials performance within the FEA framework. The CDP allows for the simultaneous simulation of cracking and crushing by defining separate stress–strain relationships and damage evolution laws for tensile and compressive behaviour [43, 60, 61].

3.2.1 Concrete damage plasticity model (CDP)

The CDP model governs the nonlinear behaviour of masonry in the continuous model (CM). Initially formulated for brittle concrete behaviour [54], CDP has proven effective in capturing the response of various brittle materials, including masonry. Lubliner [54] first introduced the CDP model as an isotropic plasticity model. Lee & Fenves [56] later improved it by incorporating stiffness recovery after crack closure under cyclic loading. The core concept of CDP lies in the distinction between tensile and compressive responses. Damage is defined based on the 'effective configuration'. This concept equates the stress state in the undamaged ($\boldsymbol{\sigma}_0$) and damaged ($\boldsymbol{\sigma}$) configurations, considering the damage parameter (d), as shown in Eq. (13). This equivalence is established under the assumption of strain equivalence, Eq. (14):

$$\sigma = d \cdot \sigma_0, \tag{13}$$

$$\varepsilon = \varepsilon_0. \tag{14}$$

Here, $\boldsymbol{\varepsilon}$ represents the total strain tensor, $\boldsymbol{\varepsilon}^e$ denotes the elastic strain component, and $\boldsymbol{\varepsilon}^p$ represents the plastic strain component, reflecting the CDP model's foundation in classical plasticity.

$$\boldsymbol{\varepsilon} = \boldsymbol{\varepsilon}^e + \boldsymbol{\varepsilon}^p \tag{15}$$

The elastic stress ($\boldsymbol{\sigma}$) is related to the elastic damage stiffness matrix ($\boldsymbol{E}$) through Hooke's Law (Eq. 16):

$$\sigma = E(\varepsilon - \varepsilon^p). \tag{16}$$

To account for damage irreversibility, the degraded stiffness matrix ($\boldsymbol{E}$) is expressed as:

$$E = (1 - d)E_0 \tag{17}$$

where E_0 represents the undamaged elastic stiffness matrix. During the elastic phase, the damage parameter (d) is zero. It progressively increases towards the value of 1 as the material approaches complete

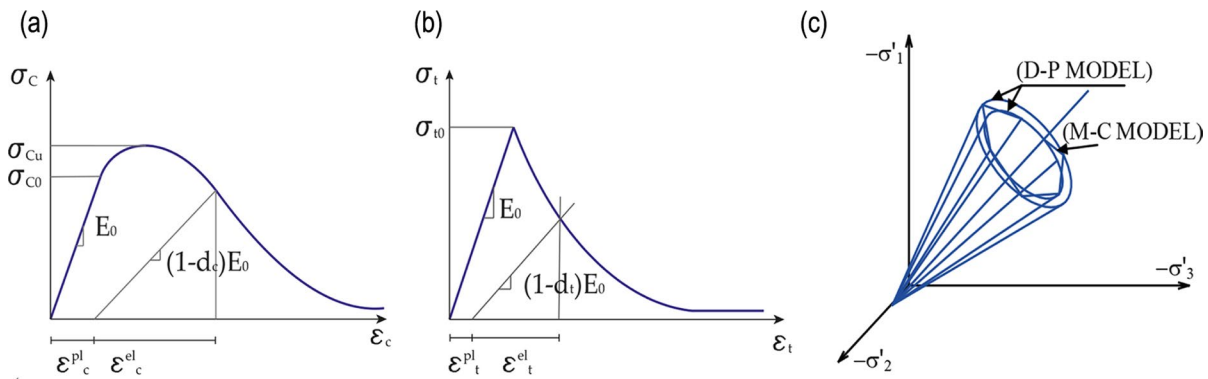

Fig. 7 Compression inelastic mono axial curve (**a**), Tensile inelastic mono axial-curve (**b**), Yield surface in the Westergaard space (**c**)

rupture. As a result, the stress–strain relationship becomes:

$$\boldsymbol{\sigma} = (1 - d)\boldsymbol{E}_0(\boldsymbol{\varepsilon} - \boldsymbol{\varepsilon}^p). \tag{18}$$

Separate damage variable laws are defined for tension and compression (Eqs. 19, 20) to capture the higher stiffness degradation in tension (σ_t) compared to compression (σ_c) under uniaxial stress (Fig. 7a–b). These damage variables increase with increasing elastic strain:

$$\sigma_t = (1 - \mathrm{d_t})E_0(\varepsilon_t - \varepsilon_t^p) \tag{19}$$

$$\sigma_c = \left(1 - d_c\right)E_0\left(\varepsilon_c - \varepsilon_c^p\right) \tag{20}$$

However, under cyclic loading, crack closure contributes to a partial recovery of elastic stiffness, especially when transitioning from tension to compression.

This phenomenon is captured by

$$(1 - d) = (1 - s\_td\_c)(1 - s\_cd\_t) \tag{21}$$

The parameters s_t and s_c are introduced to account for stiffness recovery during the load inversion stage. These factors depend on weight factors w_t and w_c, that influence the degree of stiffness recovery according to

$$s_t = 1 - w_t r^*\left(\hat{\bar{\sigma}}\right) \tag{22}$$

$$s_c = 1 - w_c\left(1 - r^*\left(\hat{\bar{\sigma}}\right)\right) \tag{23}$$

The factor $r^*\left(\hat{\bar{\sigma}}\right)$ ranges from zero to one, being zero when all principal stresses are positive and reaching one when all principal stresses are negative.

The weight factors w_t and w_c govern the extent of stiffness recovery. When they are zero, stiffness recovery is neglected. Conversely, when they are equal to one, it signifies complete recovery of stiffness.

To delineate the boundary of the elastic domain, a yield strength function based on the Drucker-Prager function is employed (as illustrated in Fig. 7c).

$$F(\bar{\boldsymbol{\sigma}}, \boldsymbol{\kappa}) = \frac{1}{1 - \alpha}\left[\alpha I_1 + \sqrt{3I_2} + \beta(\boldsymbol{\kappa})\left\langle\hat{\bar{\sigma}}_{max}\right\rangle - \gamma\left\langle-\hat{\bar{\sigma}}_{max}\right\rangle\right] - c_c(\boldsymbol{\kappa}), \tag{24}$$

where:

- I_1: First invariant of effective stress
- I_2: Second invariant of effective stress
- $\hat{\bar{\sigma}}_{max}$: Maximum principal effective stress

The constants α and $\boldsymbol{\kappa}$ are determined using the initial uniaxial compressive yield stress (f_{b0}) and the initial equiaxial compressive yield stress (f_{c0}) as:

$$\alpha = \frac{f_{b0} - f_{c0}}{2f_{b0} - f_{c0}}, \tag{25}$$

$$\beta = \frac{c_c(\boldsymbol{\kappa})}{c_t(\boldsymbol{\kappa})}(\alpha - 1) - (1 + \alpha). \tag{26}$$

Additionally, $c_c(\boldsymbol{\kappa})$ and $c_t(\boldsymbol{\kappa})$ represent the effective cohesion in compression and tension, respectively. Finally, the constant γ is calculated as:

$$\gamma = 3\frac{1 - k_c}{2k_c - 1}, \tag{27}$$

where $\mathrm{k_c} = \mathrm{I_{2,TM}}/\mathrm{I_2}, \mathrm{CM}$ is the ratio of the second stress invariants on the tensile meridian (*TM*) and compressive meridian (*CM*) at the initial yield point (Fig. 7c).

The CDP model incorporates a non-associated flow rule to govern the plastic flow direction. This means the direction of plastic strain increment may not necessarily coincide with the normal to the yield surface. The model employs the Drucker-Prager hyperbolic function to define the plastic potential (flow potential). This function is characterized by three key parameters:

- Dilatation Angle ψ: this parameter controls the volume change associated with plastic flow. A positive ψ indicates dilation (volume increase) during plastic deformation, while a negative value signifies compaction.
- Eccentricity (ε_{eccen}): This parameter influences the shape of the flow potential in the stress space. A value of $\varepsilon = 0$ results in a circular flow potential, while $\varepsilon \neq 0$ introduces eccentricity.
- Tensile Strength (f_{t0}): This parameter defines the tensile strength limit of the material.

The values of materials parameters are reported in Table 2.

Table 2 Materials parameters used in the continuous model

	Good masonry	Bad masonry
Young's Module [MPa]	1500	870
Poisson's module [-]	0.4	0.4
Weight density [kN/m^3]	18	19
Strength in compression [MPa]	2.2	1.0
Strength in tension [MPa]	0.22	0.19
Dilatation angle,ψ	13°	
Correction parameter,k_c	0.666	
Eccentricity,ε_{eccen}	0.2	
Biaxial strength ratio,f_{b0}/f_{c0}	1.16	
Viscosity	0.002	

4 Numerical analysis

The structural dynamic response of this religious building was investigated through nonlinear dynamic analyses using numerical models. Initially, the structure was influenced only by gravitational forces, followed by the application of the seismic sequence of central Italy 2016, consisting in four significant events recorded between August 24th and October 30th.

The seismic sequence is selected considering that the damage pattern currently visible is the result of a prolonged sequence. As a result, the damage activation might be demanding to define 'a priori'. By employing this approach, it could be possible to replicate a more realistic scenario, thereby allowing a better understanding of the pros and cons about the method applied, and in relation to a potential evolution of the damage itself.

Data were collected from the reference station placed in Matelica (MTL) within the Italian Accelerometric Archive (ITACA) database (Fig. 8). Those earthquakes were applied sequentially to account for a cumulative damage. To reduce computational burden, for each event, only the 10-s time around the highest peaks and 2 s of null acceleration between consecutive shocks were encompassed, resulting in a total investigation duration of 46 s. The step-time increment was assumed for a value of 0.005 s, considering the accelerograms in the three spatial directions (north–south, east–west, and vertical). Table 3 presents key data for the four analysed seismic events, including:

- EC8 class: the type of ground on which the earthquake was recorded
- R_{jb}: Joyner-Boore distance, which is the distance to the nearest point on the surface projection of the fault
- R_{rup}: minimum distance between the site and the fault
- R_{epi}: the epicentral distance (geometrically calculated distance)

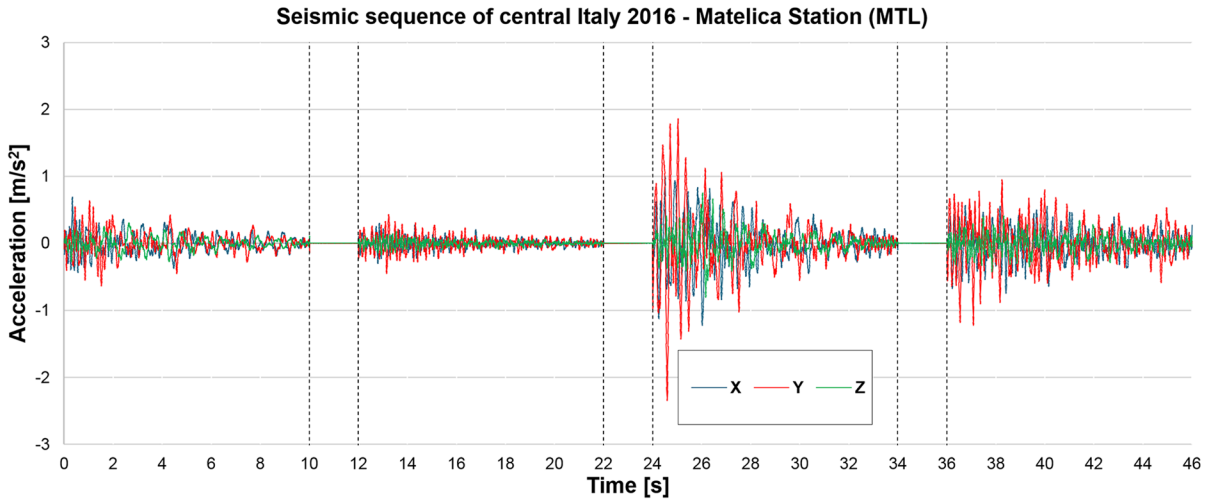

Fig. 8 Seismic sequence applied for the nonlinear dynamic analysis, recorded in Matelica (MTL)

Table 3 The main characteristics of the four quakes implemented in the modal analysis

Seismic event	M_L	Depth [km]	Station	Class EC8[a]	R_{jb} [km]	R_{rup} [km]	R_{epi} [km]	NS PGA [cm/s^2]	EW PGA [cm/s^2]	U PGA [cm/s^2]
24/08/2016 (01:36:32)	6.00	63.90	MTL	B	44.49	44.49	63.90	− 66.71	69.95	31.02
26/10/2016 (17:10:36)	5.40	42.70	MTL	B	39.64	40.08	42.70	− 44.58	− 30.00	17.63
26/10/2016 (19:18:06)	5.90	39.10	MTL	B	28.18	28.19	39.10	− 240.47	− 122.18	− 77.86
30/10/2016 (06:40:18)	6.10	47.10	MTL	B	35.33	35.32	47.10	− 122.44	75.96	− 44.08

[a]Classification of site not based on direct measure of $V_{s,30}$

5 Numerical results

In this paragraph, are examined the numerical modelling outcomes obtained using the discontinuous and continuous models under investigation in this research for the Church of San Nicolò in Sentino.

Six control points have the same coordinates in both models (Fig. 9). The first point P_1 is located at the top of the main façade, points P_2 and P_4 are situated on the respective spine walls of the main façade, while point P_3 is placed on the southeast façade. Finally, the remaining monitoring points, P_5 and P_6, are located at the top of the bell tower. The results of the different models are reported in terms of the displacement of six control points (Table 4) with respect to the Time Histories in the x, y, and z directions (Fig. 10), as well as in terms of block sliding damage and masonry tensile damage (Fig. 11).

The comparison between the numerical results of the models with the existing crack pattern assists in the thoroughly investigation of the dynamic response of the church during the 2016 Central Italy seismic sequence and to evaluate the correlation between the real damage of the structure and the response of the models.

In the continuous model, the structure remains nearly intact after the initial 10 s: indeed, the displacements remain close to zero until just before the final two events.

On the other hand, the discrete element models report significant involvement in the bell tower area, detecting displacements of the order of centimetres in the x-direction for the bell tower and the church structure. Specifically, after the first shock in the NSCD and DEM models, the displacements of P_1, P_2, P_3, and P_4 in the x and y directions are similar, while the values of the remaining monitoring points in the bell tower differ slightly between the two methods.

At the end of the first sequence, the most significant displacements along x/y are found in the discontinuous model: point P_2 has values of − 11.1 mm/ − 5.5 mm in 3DEC, − 12. mm/ − 5.0 mm in LMGC90, as well as P_6 in the bell tower with residual displacements of − 11.3 mm/ − 1.6 mm in 3DEC, − 12.3 mm/ − 2.7 mm in LMGC90.

The second seismic event (26th October 2016 – 17:10), owing to the lower magnitude, provides minimal change in terms of damage and

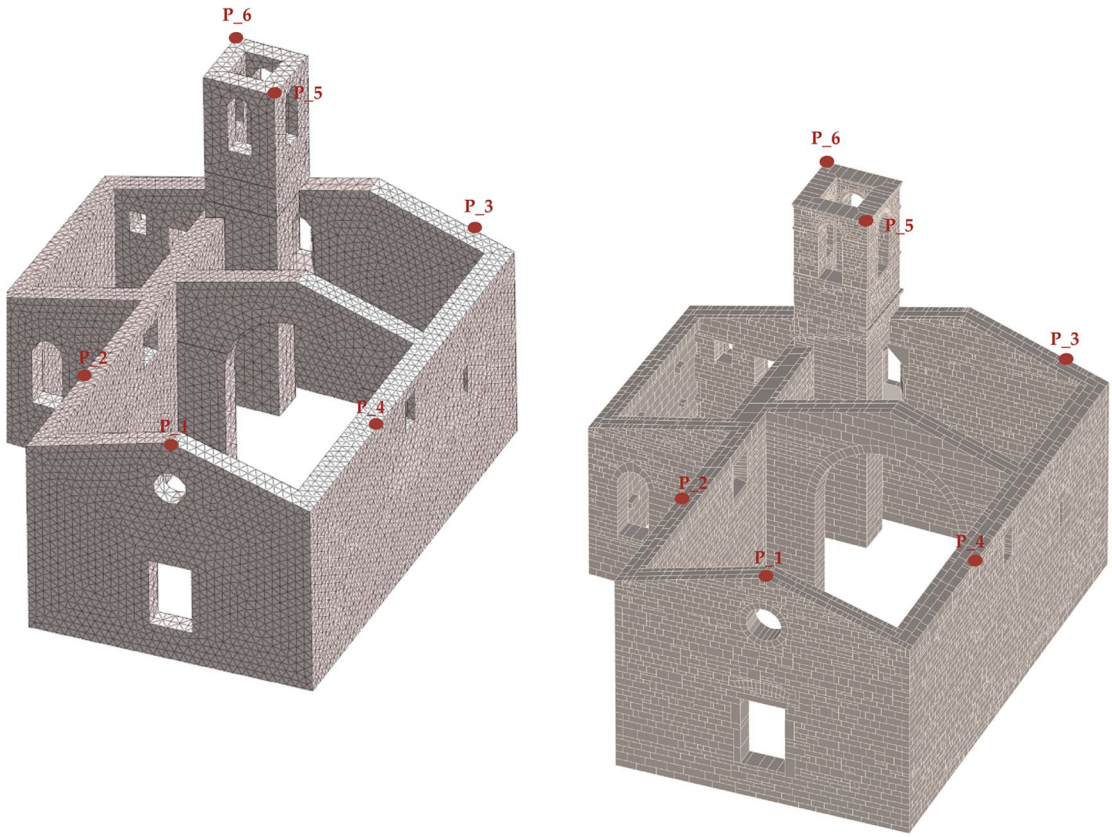

Fig. 9 Finite element (left) and discrete element (right) models with control points used in subsequent nonlinear dynamic analyses

displacements. During this acceleration, the structural scenario has remained unchanged in the discrete model, while in the CDP, as confirmed by Fig. 11, the tensile damage has increased at the base of the bell tower, as stress concentration loci, thereby contributing to the expansion of the existing crack pattern.

Nevertheless, the most extensive damage was observed for the last two events, characterized by more tensile damage in the continuous approach and greater displacements of the blocks in the discontinuous ones. Indeed, they accounted for maximum values 20 mm in the bell tower that resulted the most affected by these shocks, demonstrating to be the most vulnerable element in both the Discrete Element Method and the Non-Smooth Contact Dynamics (Fig. 11). The belfry cell exhibited deterioration in the openings, on the northwest and northeast façades, where there is evidence in the keystone dropping of the openings and in the sliding of the adjacent blocks. At the end of the 36-s simulation with the LMGC90 software, the damage of the arch was observed, providing the collapse of several voussoirs on the northeast façade of the bell tower, a mechanism not observed in the actual structure (Fig. 12).

In the model investigated with the CDP, after 34 s, substantial displacements along the x/y axes were detected in the church structure. In particular, the most notable ones were recorded along x-direction at points P_2 (−11.6 mm) and P_4 (18.4 mm). This behaviour is also evident in the tensile damage pattern, where the structure appears much more cracked than in the previous event, showing vertical and diagonal cracks at the openings and wall connections. In addition, the volume of tensile damage in the masonry in the CDP model in this scenario accounts for a value of 29.2% compared to 2.1% from the previous earthquake, highlighting the significant impact of the third event on the structure.

The fourth seismic event examined (30th October) has increased the existing crack condition in

Table 4 Displacement values recorded for each control point for MTL seismic sequence

	Time	P_1			P_2			P_3			P_4			P_5			P_6		
		X	Y	Z	X	Y	Z	X	Y	Z	X	Y	Z	X	Y	Z	X	Y	Z
	[s]	[mm]			[mm]			[mm]			[mm]			[mm]			[mm]		
DEM	10	−10.4	−6.3	1.2	−11.1	−5.5	1.2	−10.1	−4.9	1.2	−10.1	−5.4	1.3	−6.5	−10.0	−0.2	−11.3	−1.6	0.1
	22	−9.6	−6.0	1.2	−10.0	−5.6	1.3	−9.4	−4.6	1.3	−8.7	−5.6	1.3	−5.6	−9.9	0.0	−10.3	−0.8	0.2
	34	−6.9	−5.4	−6.9	−5.0	−2.7	−6.0	−2.9	4.4	−6.2	−2.5	−1.6	−6.1	18.5	−14.6	−8.2	−17.3	33.6	−9.4
	46	−5.0	−12.7	−3.2	−3.3	−3.0	−1.8	−1.9	4.0	−2.0	−1.7	−1.8	−2.0	22.3	−21.5	−4.4	−17.4	34.1	−5.2
NSCD	10	−10.4	−4.5	1.4	−12.2	−5.0	1.5	−10.1	−4.5	1.6	−11.9	−5.1	1.6	−8.6	−5.5	0.8	−12.3	−2.7	0.2
	22	−9.6	−7.3	1.3	−9.8	−5.2	1.6	−9.4	−5.1	1.7	−9.1	−5.2	1.6	−8.2	−5.0	1.0	−11.9	1.1	−0.1
	34	−5.2	0.3	−7.3	−5.7	1.6	−5.9	−2.7	3.6	−5.8	−6.0	1.2	−5.9	−3.0	−10.0	−6.7	−21.6	14.9	−8.4
	46	−3.9	0.3	−3.8	−3.6	2.0	−2.1	−1.5	3.2	−2.0	−4.3	1.6	−2.1	−1.6	−9.6	−2.3	−30.3	23.5	−5.4
CDP	10	−0.4	−0.2	−0.4	−0.8	0.1	−0.5	−0.1	0.5	−0.5	−0.5	0.1	−0.4	−1.0	1.0	0.0	−0.9	1.1	−0.4
	22	−0.9	−0.5	−0.8	−1.4	−0.3	−0.8	−0.6	0.3	−0.9	−1.0	−0.2	−0.7	−1.5	1.2	−0.1	−1.7	0.9	−0.8
	34	−0.2	−21.1	−1.0	−11.6	−9.5	−0.2	−0.6	7.1	−3.6	18.4	−7.3	−1.6	2.8	49.3	27.1	1.2	47.7	15.9
	46	−3.2	−35.3	−3.1	−21.7	−19.8	−1.6	−5.2	1.1	−7.3	20.2	−17.3	−4.2	−7.5	70.3	46.1	−7.3	70.5	22.0

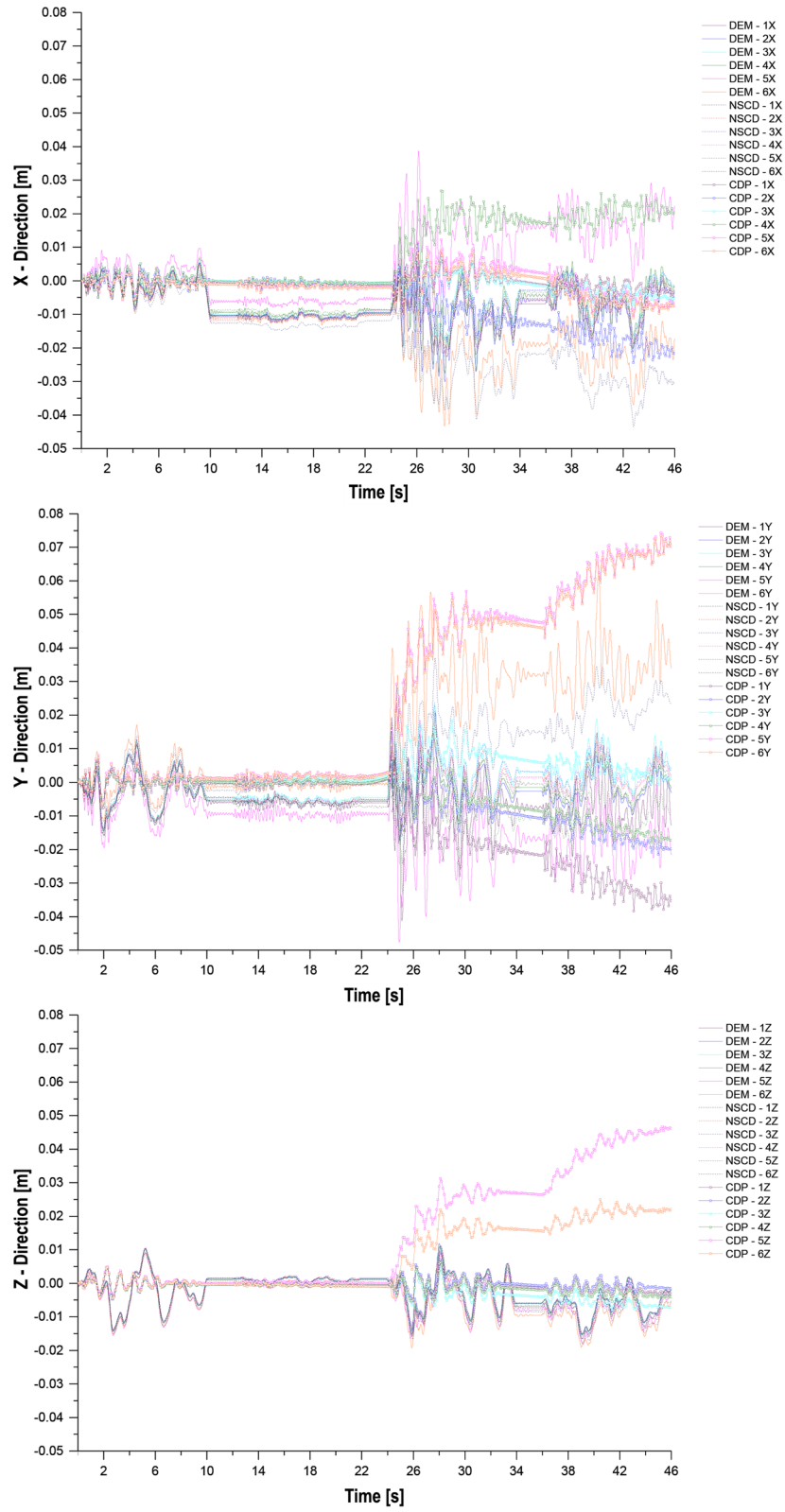

Fig. 10 Displacements' time histories of the six control points used (Seismic station MTL—Matelica)

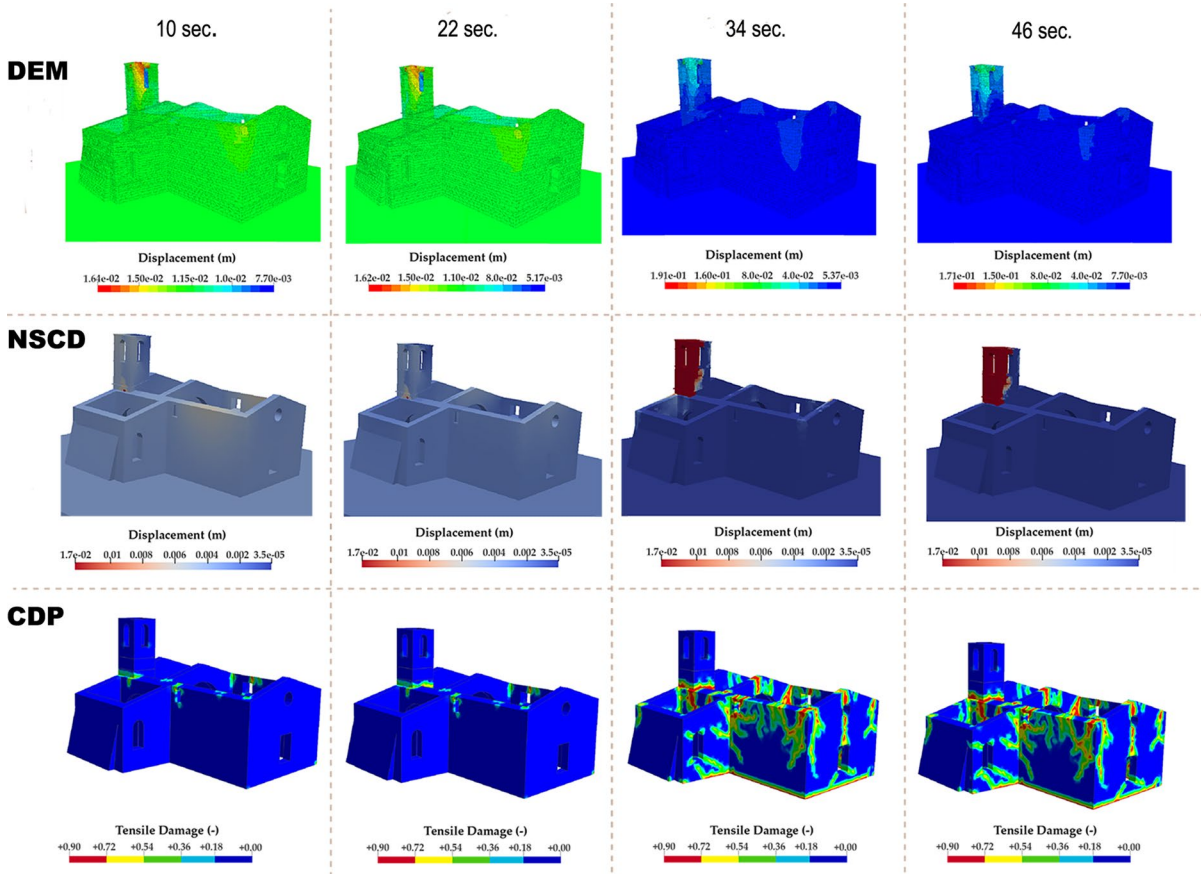

Fig. 11 Numerical damage at the end of each seismic shock in the considered sequence in terms of displacement for DEM and NSCD, and tensile damage for CDP

the continuous model, in which the primary damage occurred in the church's façade and nave walls, resulting a tensile damage volume of 30.4%. Substantial displacements in the x/y direction at monitoring points P_2 (−21.7 mm/−19.8 mm) and P_4 (20.2 mm/−17.3 mm) were recorded, suggesting a potential combined overturning mechanism, as indicated by the diagonal cracks developed both in the actual state of the church and in the continuous model.

Moreover, notable displacements are observed in the y-direction (70 mm) of the bell tower control point (P_5 and P_6). Likewise, in the discontinuous models, the most several effects were reported in the bell tower, where maximum displacements after the last shock in both the DMs were concentrated, getting worse its instability.

There is also evidence of very slight deviations between the x and y directions (Table 4) in all displacements for both discontinuous methods (DEM and NSCD), except at the bell tower control points. Regarding the z direction, the values obtained in the discontinuous models could be comparable.

It is worthy to underline that, in the CDP modelling, an increase of residual displacements is detected from the 24th to the 46th second. On the other hand, no significant residual displacements are observed in the DMs. This discrepancy in behaviour can be attributed to the different nonlinear governing laws characterizing each approach. Finally, the last two seismic events induce the most substantial displacements across all the models.

Nevertheless, the differences between DEM and NSCD methods can be noted by observing

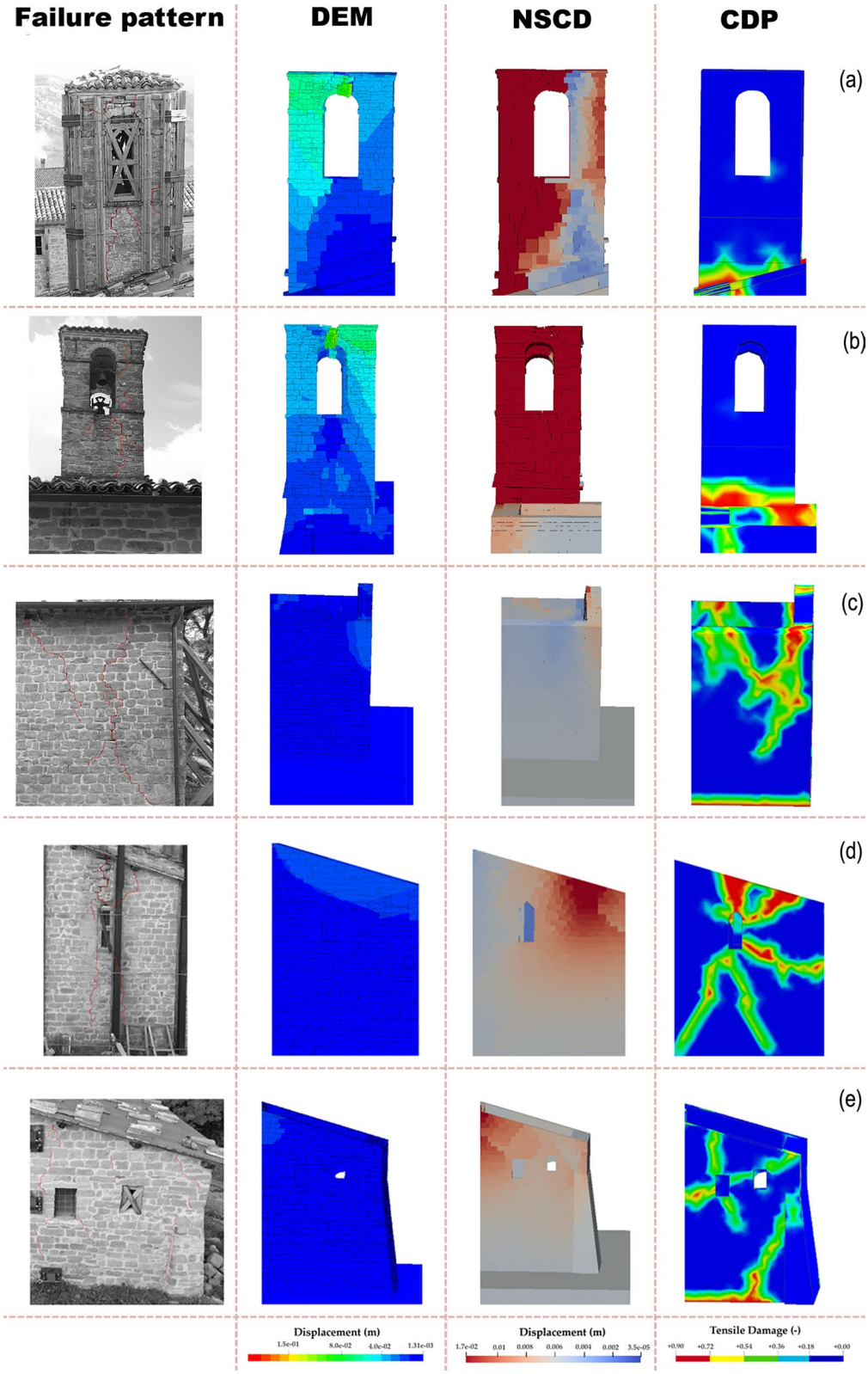
Failure pattern
DEM
NSCD
CDP
(a)
(b)
(c)
(d)
(e)
Displacement (m)
1.5e-01
8.0e-02
4.0e-02
1.31e-03
Displacement (m)
1.7e-02
0.01
0.008
0.006
0.004
0.002
3.5e-05
Tensile Damage (-)
+0.90
+0.72
+0.54
+0.36
+0.18
+0.00

◂**Fig. 12** Comparison between the numerical and real damages after the seismic sequence of central Italy in 2016

the oscillations in all three directions, in particular after 24 s, due to the laws governing the contacts between the blocks and the diverse behaviours in stabilising residual displacements. In the DEM method, the 'smooth' contact laws between the blocks are perfectly elastic. Therefore, even for small displacements, there is evidence in recording significant oscillations of the DEM blocks that result also larger compared to the other NSCD method. In addition, oscillations are registered during the 2-s pause period between one another seismic sequence, although free from any acceleration. Conversely, the NSCD model features 'non-smooth' inelastic impacts between the blocks, resulting in no recoil or rebound phenomena post-impact. In this case, the onset of displacement begins at the debonding load point, depending on the friction law. In conclusion, the initial shocks indicated that the bell tower is the most vulnerable element in the discontinuous model. The displacements at P_6, located at the top of the bell chamber, show significant and similar values in both the DEM and NSCD models compared to the church's underlying structure. In the continuous model, however, displacements are nearly zero.

The latest seismic events have amplified the crack pattern in the bell tower for the discontinuous model, as underlined by increased displacements of the control points at the end of the sequence and by the evolution of the damage where greater block sliding is observed. On the other hand, in the CDP model, the tensile damage is mainly concentrated in the church structure. In particular, the activation of the out-of-plane overturning mechanism of the main façade is confirmed by the maximum displacements accounting for values at the control point as previous reported.

Finally, the numerical damage assessments from different models are compared with the actual structural damage (Fig. 12). Each model effectively replicates the existing crack patterns in the structure, according to their respective capabilities. The discrete element model accurately describes the crack pattern in the bell tower, while the finite element model shows the bell tower exhibiting cantilever-like behaviour with localized damage at its base. The continuous model provides a more detailed representation of the diagonal failures, observed in the northeast façade.

5.1 Numerical damage and real structural crumbling comparison

The simulation results were compared with the actual damage to the structure, demonstrating how different approaches in constitutive laws are crucial for investigating masonry vulnerability and providing a comprehensive understanding of the structure's dynamic behaviour. After 46 s of simulation, the northwest façade of the bell tower in the discontinuous models aligns with the existing crack pattern (Fig. 12a). The failure mechanism of the bell chamber opening and the developing of various vertical cracks along the façade are clearly evident. Conversely, the bell chamber in the continuous model performed like a cantilever beam, resulting in damage patterns differing from the current condition of the structure. The northeast façade of the bell tower also demonstrated realistic behaviour in the discontinuous approach, in particular in the DEM model, where block sliding follows the existing crack pattern of the structure (Fig. 12b). In the NSCD model, block displacements were larger and more significant than in the DEM model, resulting in the collapse of two blocks at the top of the bell tower that is not comparable with the real structural behaviour after the seismic sequences. In the continuous model, the bell tower failures corresponding to the joint with the church structure, as previously described. Considering the main façade, it is important to underline that its activation of the combined overturning mechanism is highlighted by cracks and displacements in all the three models, especially in the continuous method, where cracks conform to the existing pattern of the orthogonal walls to the main façade (Fig. 12c). Regarding the southeast façade, the sliding of blocks above the 'monofora' was captured through the three models, thanks to the tensile cracks in the continuous model and the block displacements in the discontinuous approach (Fig. 12d). Similarly, quasi-vertical cracks propagating from the upper part of openings in the southeast façade could be more detected in the NSCD model and in the CDP one (Fig. 12e). Finally, although with different methodologies, there is evidence in a better handling of nonlinear behaviour by the NSCD and CDP approaches, in

particular for the simulations of cracks formation and discontinuities managing.

However, the collapse of the external wall of the northeast façade of the sacristy was not reported by the continuous models. This might be depending on a combination of factors, including the influence of the site distance to the seismic station, where accelerations and velocities were registered for the simulation. Data recorded in Camerino station, closer to the 2016 epicentres than Matelica station, would have provided more accurate results. Despite these factors and various modelling approximations, the overall outcomes could be overlapped to the actual damage observed.

5.2 Numerical simulations through the main seismic events of the Central Italy 2016 earthquake sequence

For the sake of completeness, considering that the accelerations recorded in Matelica station are lower than those effective in situ, these numerical simulations were also carried out using the time history data recorded in the seismic stations closer to the epicentral point (Fig. 13) [62]. These analyses were implemented to evaluate in-depth the damage development of that religious masonry building under investigation.

Firstly, in Fig. 14 there is a clear correspondence between the discontinuous models, the 'DEM' and the 'NSCD'. Indeed, the belfry collapse could be observed for both the DM methods, meanwhile in the

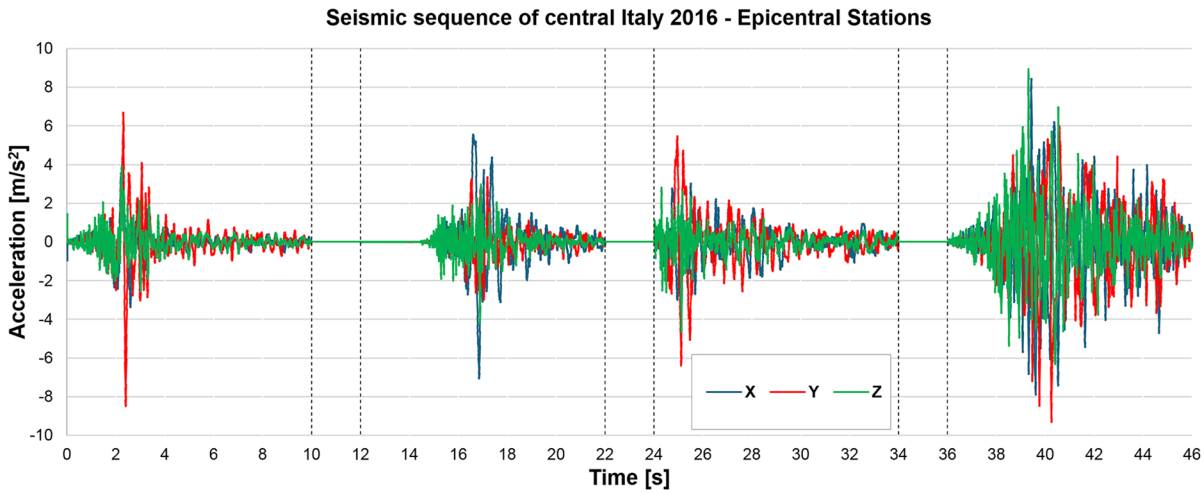

Fig. 13 Accelerations recorded in the epicentral stations

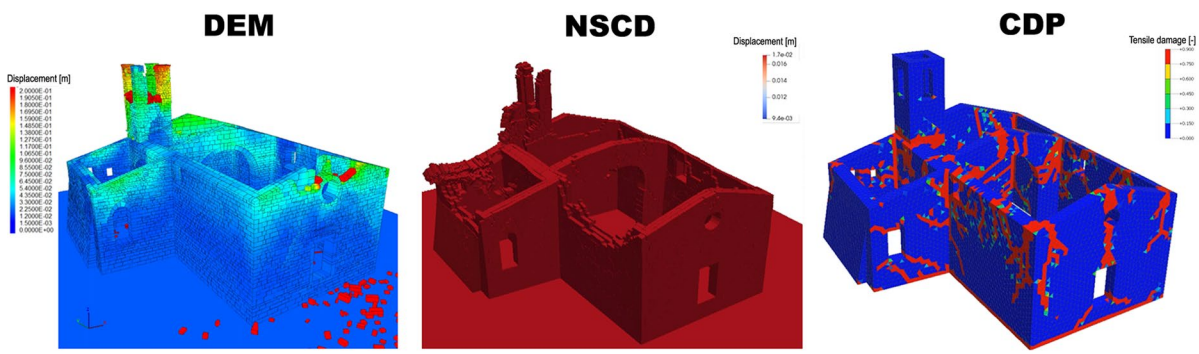

Fig. 14 Global view of the damage at the end of the analysis with epicentral actions

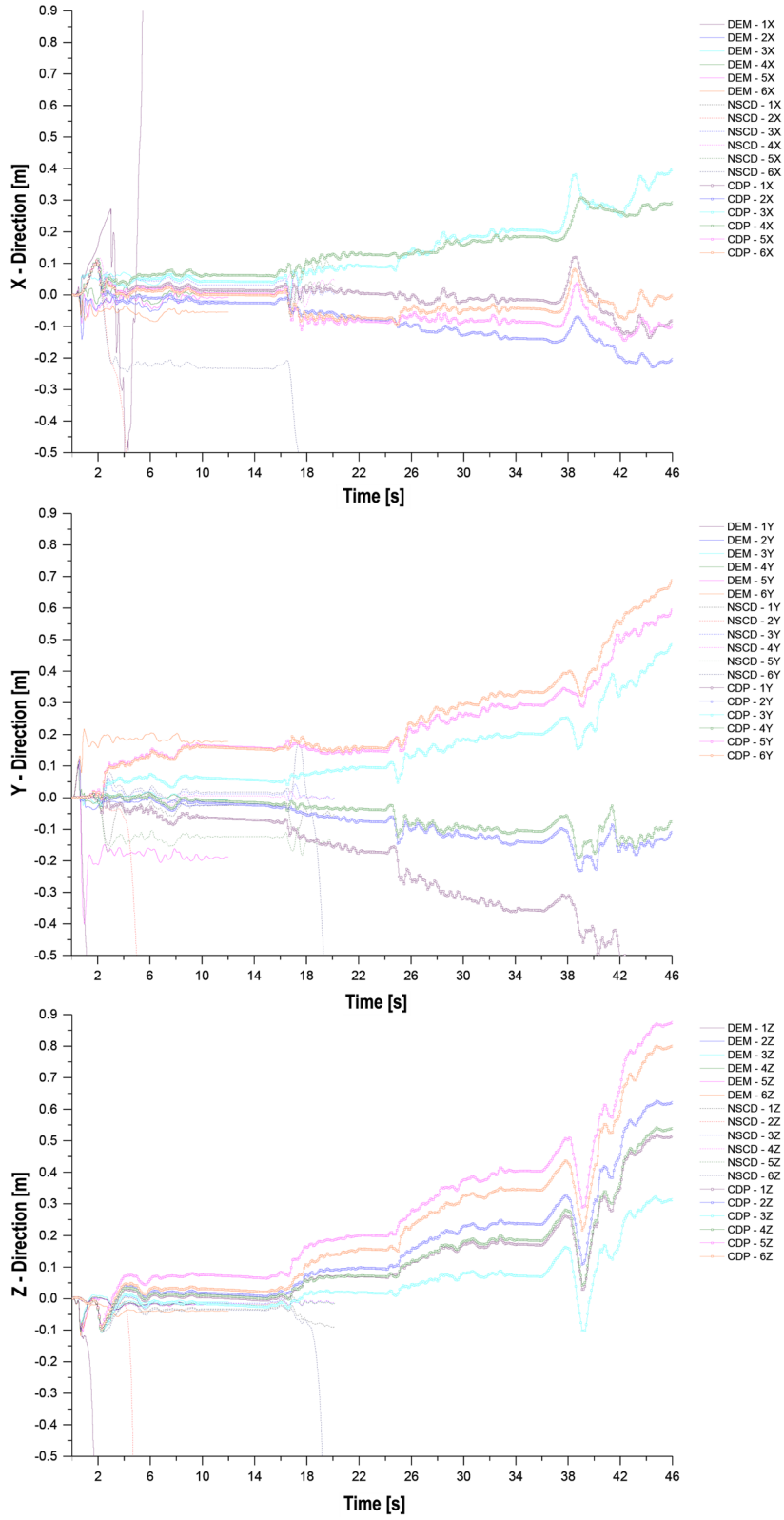

Fig. 15 Displacements' time histories of the six control points used with epicentral actions

CDP model was not displayed at all even at the end of the last sequence at the 46th second, as reported in Fig. 15 in terms of displacements of the same control points of Fig. 9.

For the DEM model, there is evidence in the overturning mechanism of the upper part of the main façade, just above the rose window. Conversely, the NSCD displayed general dislocations in the rear part of the building. In this case, the external wall collapse of the sacristy could be observed, even after the first seismic sequence of 10 s. Likewise, in this model, the collapse of both the walls of the nave was detected. Indeed, the failure pattern underlines the trigger of the out-of-place mechanism.

Moreover, a good comparison between the NSCD model to the CM up to the end of the second sequence (20th second) is highlighted: the collapse of the bell tower, the lateral nave and the external wall of the sacristy could be confirmed thanks to the continuous model.

Finally, it is worthy to underline that the DM simulations automatically stop as soon as collapse occurs due to the lack of convergence in the numerical solution. Only FEM analysis can continue, thanks to its homogenization properties, until the end of the fourth seismic shock, at the 46th second (Fig. 15).

6 Conclusions

In this research, the assessment of the 'San Nicolò' Church, located in Sentino, a hamlet of Camerino is illustrated through numerical simulations. This building can be considered a symbol for the significant damage subjected after the Central Italy earthquake of 2016 and 2017, due to its proximity to the epicentres of the seismic sequence affecting the Apennine region.

The response to seismic activity of this religious building was studied using nonlinear dynamic analyses with both continuous and discontinuous approaches. The continuous approach modelled the masonry as an isotropic and homogeneous material, while the discontinuous method considered it as an assembly of three-dimensional individual blocks, incorporating mortar characteristics and interaction laws.

To analyse the structural response, both models were implemented to nonlinear dynamic assessments, sequentially undergoing the four main shocks of the earthquake swarm. Displacement data from various points indicated similar results between the two modelling approaches. However, comparing the numerical outcomes to the actual damage observed, it is clear that both models could replicate the failure pattern developed in the church, although with varying degrees of accuracy. The continuous model is effective when the structural response does not depend on the masonry texture. Conversely, discrete models provided more consistent results in regions, such as the Apennine ones, characterized by buildings with irregular masonry, due to the challenges in defining the critical role of the block-to-block interaction.

The seismic actions of interest, recorded near the case study, were applied to the base of the models, considering only the 10 s of peak maximum for each event, with a two-second pause between them, to reduce the computational time. In detail, accelerograms in the discontinuous methods and in the CDP method were used in the three spatial directions, evaluating the vulnerability of the case study.

From the comparison of the different approaches used, it emerged that both were able to replicate, according to their characteristics, the existing failures pattern of the religious building and the activation of mechanisms. The continuous model highlights in-plane mechanisms in the walls, while the discontinuous one allows for the analysis of rotations and detachments between blocks, up to the collapse of the masonry.

The numerical results obtained were significant for assessing the vulnerability of the masonry structure. The discontinuous approach demonstrated that the most damaged and fractured points were those on the bell tower; indeed, they exhibited the greatest displacement at the end of the simulation. This outcome aligns with the real crack pattern of the bell cell, characterized in some points by almost disintegrated masonry.

Despite the bell tower being the most vulnerable element, the cracks observed in the bell tower in the CDP model differ from the actual condition. The bell tower behaves like a cantilever beam, with the cracks localized at the connection with the main body of the church and, therefore, performing smaller displacements compared to the other two methods. The crack pattern, in this case, was better described by the discontinuous model.

Another vulnerable point highlighted through these approaches, and in particular by the Concrete Damage Plasticity method, is the main façade of the church. The diagonal passing cracks developed in the main façade walls are a clear symptom of the activation of the combined overturning mechanism. Indeed, especially in the continuous model, the displacements of control points P_1, P_2, and P_4 and the highlighted cracks confirm this.

Therefore, the numerical results demonstrated that DMs better replicated the bell tower damage response; on the other hand, the CM reproduced more clearly the diagonal cracks in the northeast façade. Then, both approaches accurately simulated the in-plane cracks, visible near the 'monofora' and the openings.

Finally, the numerical results obtained from different simulations, along with their diverse approach properties, highlights the scientific relevance of this document. The findings of this study illustrate that none of the methodologies employed is capable of accurately representing the overall damage to such complex buildings. These types of cultural sites are distinguished not only by their irregular geometry in all directions but also by structural modifications and changes in use that have affected their masses and stiffness, making them especially challenging to assess through the application of traditional methods. It can be concluded that the optimal solution is the intelligent integration of each method. For instance, the CDP should be employed for preliminary and global simulations of the building to establish the primary location at which a local mechanism may potentially become activated. Furthermore, the CDP may be employed to define the behaviour at the point of collapse. It is evident that this approach is not viable for weaker actions due to the intrinsic material properties and conditions of homogeneity. However, it may be more appropriate for residuals, as demonstrated above.

Conversely, DMs are well suited to modelling simulations of local mechanisms. Due to the intrinsic material properties of the material, the displacements are accurately reported for the damage of a single structural member, even in the initial sequence, while the damage is only slightly activated.

Accordingly, an optimal compromise could be developed to facilitate the analysis and reduce the computational burden. Therefore, it is the aim of this research to propose the application of a potential procedure that could evolve into a reliable and suitable methodology for the overall prediction of failure scenarios and structural damage in the case study under lateral loading conditions, aligned with the current state of knowledge and exploiting the advantages of each method. To elaborate further, that potential procedure might suggest, following the initial implementation of a CM approach for the structural building as a whole, to concentrate on the particular structural members by means of DM, that may encompass those deemed responsible for the irregularities observed in the buildings.

Acknowledgements The authors express their gratitude to Itasca Harpaceas for providing access and support for 3DEC© under the IEP program as well as the Italian Ministry of University (Italy) for the support under the program "Dipartimento di Eccellenza" of the Department of Civil and Building Engineering, and Architecture—Polytechnic University of Marche (Ancona, Italy). The authors gratefully acknowledge the WP4 line "MARS - CARTIS" of the DPC-ReLUIS 2024–2026 research project for providing financial support for the development of this work. Finally, the second author is grateful to the European Union-NextGenerationEU along with the Italian Ministry of University and Research (Italy) for funding the research program 'L.A.ST.ING.' (ID grant: MSCA_0000036), under the National Recovery and Resilience Plan (NRRP), according to the Mission 4, "Education and Research"—Component 2, "From Research to Business", Investment 1.2, "Funding projects presented by young researchers" (MSCA grants), in order to carry on the research activities on the present topic.

Author contributions Mattia Schiavoni: Visualization, Data curation, Investigation, Formal analysis, Validation, Software, Methodology. Francesca Roscini: Investigation, Formal analysis, Data curation, Writing—original draft, Writing—review & editing, Validation, Methodology, Conceptualization. Francesco Clementi: Investigation, Supervision, Writing—review & editing, Validation, Methodology, Conceptualization.

Funding Open access funding provided by Università Politecnica delle Marche within the CRUI-CARE Agreement.

Data availability No datasets were generated or analysed during the current study.

Declarations

Conflict of interest The authors declare no competing interests.

References

1. Lagomarsino S (2006) On the vulnerability assessment of monumental buildings. Bull Earthq Eng 4:445–463. https://doi.org/10.1007/s10518-006-9025-y
2. Malena M, Portioli F, Gagliardo R et al (2019) Collapse mechanism analysis of historic masonry structures subjected to lateral loads: a comparison between continuous and discrete models. Comput Struct 220:14–31. https://doi.org/10.1016/j.compstruc.2019.04.005
3. Mallardo V, Malvezzi R, Milani E, Milani G (2008) Seismic vulnerability of historical masonry buildings: a case study in Ferrara. Eng Struct 30:2223–2241. https://doi.org/10.1016/j.engstruct.2007.11.006
4. Milani G (2013) Lesson learned after the Emilia-Romagna, Italy, 20–29 May 2012 earthquakes: a limit analysis insight on three masonry churches. Eng Fail Anal 34:761–778. https://doi.org/10.1016/j.engfailanal.2013.01.001
5. Sorrentino L, Cattari S, da Porto F et al (2019) Seismic behaviour of ordinary masonry buildings during the 2016 central Italy earthquakes. Bull Earthq Eng 17:5583–5607. https://doi.org/10.1007/s10518-018-0370-4
6. Bartoli G, Betti M, Vignoli A (2016) A numerical study on seismic risk assessment of historic masonry towers: a case study in San Gimignano. Bull Earthq Eng 14:1475–1518. https://doi.org/10.1007/s10518-016-9892-9
7. Cavalagli N, Comanducci G, Ubertini F (2018) Earthquake-induced damage detection in a monumental masonry bell-tower using long-term dynamic monitoring data. J Earthq Eng 22:96–119. https://doi.org/10.1080/13632469.2017.1323048
8. García-Macías E, Ubertini F (2019) Seismic interferometry for earthquake-induced damage identification in historic masonry towers. Mech Syst Signal Process 132:380–404. https://doi.org/10.1016/j.ymssp.2019.06.037
9. Ceci AM, Contento A, Fanale L et al (2010) Structural performance of the historic and modern buildings of the University of L'Aquila during the seismic events of April 2009. Eng Struct 32:1899–1924. https://doi.org/10.1016/j.engstruct.2009.12.023
10. Acito M, Bocciarelli M, Chesi C, Milani G (2014) Collapse of the clock tower in finale Emilia after the May 2012 Emilia Romagna earthquake sequence: numerical insight. Eng Struct 72:70–91. https://doi.org/10.1016/j.engstruct.2014.04.026
11. Valente M, Milani G (2016) Non-linear dynamic and static analyses on eight historical masonry towers in the North-East of Italy. Eng Struct 114:241–270. https://doi.org/10.1016/j.engstruct.2016.02.004
12. Asteris PG, Sarhosis V, Mohebkhah A et al (2015) Numerical modeling of historic masonry structures. In: Asteris P, Plevris V (eds) Handbook of research on seismic assessment and rehabilitation of historic structures. IGI Global, Hershey, pp 213–256
13. Giordano E, Marcheggiani L, Formisano A, Clementi F (2022) Application of a non-invasive technique for the preservation of a fortified masonry tower. Infrastructures (Basel). https://doi.org/10.3390/infrastructures7030030
14. Clementi F, Gazzani V, Poiani M et al (2018) Seismic assessment of a monumental building through nonlinear analyses of a 3D solid model. J Earthq Eng. https://doi.org/10.1080/13632469.2017.1297268
15. Clementi F (2021) Failure analysis of apennine masonry churches severely damaged during the 2016 central Italy seismic sequence. Buildings. https://doi.org/10.3390/buildings11020058
16. Clementi F, Formisano A, Milani G, Ubertini F (2021) Structural health monitoring of architectural heritage: from the past to the future advances. Int J Archit Herit. https://doi.org/10.1080/15583058.2021.1879499
17. Adam JM, Betti M, Clementi F, Ivorra S (2022) Structural health monitoring and NDT of masonry structures: research and practice. Constr Build Mater. https://doi.org/10.1016/j.conbuildmat.2021.125704
18. Betti M, Vignoli A (2011) Numerical assessment of the static and seismic behaviour of the basilica of Santa Maria all'Impruneta (Italy). Constr Build Mater 25:4308–4324. https://doi.org/10.1016/j.conbuildmat.2010.12.028
19. Poiani M, Gazzani V, Clementi F, et al (2018) Iconic crumbling of the clock tower in Amatrice after 2016 central Italy seismic sequence: advanced numerical insight. In: Procedia structural integrity. https://doi.org/10.1016/j.prostr.2018.11.041
20. Clementi F, Pierdicca A, Milani G, et al (2018) Numerical model upgrading of ancient bell towers monitored with a wired sensors network. In: Proceedings of the international masonry society conferences
21. Gazzani V, Poiani M, Clementi F, et al (2018) Modal parameters identification with environmental tests and advanced numerical analyses for masonry bell towers: A meaningful case study. In: Procedia structural integrity. https://doi.org/10.1016/j.prostr.2018.11.040
22. Quagliarini E, Maracchini G, Clementi F (2017) Uses and limits of the equivalent frame model on existing unreinforced masonry buildings for assessing their seismic risk: a review. J Build Eng. https://doi.org/10.1016/j.jobe.2017.03.004
23. Giordano E, Clementi F, Nespeca A, Lenci S (2019) Damage assessment by numerical modeling of sant'agostino's sanctuary in offida during the central Italy 2016–2017 seismic sequence. Front Built Environ. https://doi.org/10.3389/fbuil.2018.00087
24. Castellazzi G, Altri AMD, De MS, Ubertini F (2017) An innovative numerical modeling strategy for the structural analysis of historical monumental buildings. Eng Struct 132:229–248. https://doi.org/10.1016/j.engstruct.2016.11.032

25. Sarhosis V, Lemos JV, Bagi K (2019) Discrete element modeling. In: Numerical modeling of masonry and historical structures. Elsevier, pp 469–501
26. Monchetti S, Viscardi C, Betti M, Clementi F (2023) Comparison between Bayesian updating and approximate Bayesian computation for model identification of masonry towers through dynamic data. Bull Earthq Eng. https://doi.org/10.1007/s10518-023-01670-6
27. Salachoris GP, Standoli G, Betti M et al (2023) Evolutionary numerical model for cultural heritage structures via genetic algorithms: a case study in central Italy. Bull Earthq Eng. https://doi.org/10.1007/s10518-023-01615-z
28. Addessi D, Mastrandrea A, Sacco E (2014) A force-based equivalent frame element for push-over analysis of masonry structures. Key Eng Mater 624:405–412. https://doi.org/10.4028/www.scientific.net/KEM.624.405
29. Addessi D, Sacco E, Paolone A (2010) Cosserat model for periodic masonry deduced by nonlinear homogenization. Euro J Mech, A/Solids 29:724–737. https://doi.org/10.1016/j.euromechsol.2010.03.001
30. Lemos JV (2007) Discrete element modeling of masonry structures. Int J Architect Heritage 1:190–213. https://doi.org/10.1080/15583050601176868
31. Psycharis IN, Lemos JV, Papastamatiou DY et al (2003) numerical study of the seismic behaviour of a part of the parthenon pronaos. Earthq Eng Struct Dyn 32:2063–2084. https://doi.org/10.1002/eqe.315
32. Lourenço PB, Rots JG (1997) Multisurface interface model for analysis of masonry structures. J Eng Mech 123:660–668. https://doi.org/10.1061/(ASCE)0733-9399(1997)123:7(660)
33. D'Altri AM, Sarhosis V, Milani G et al (2019) Modeling strategies for the computational analysis of unreinforced masonry structures: review and classification. Arch Comput Methods Eng. https://doi.org/10.1007/s11831-019-09351-x
34. Lourenço PB (2013) Computational strategies for masonry structures : multi-scale modeling, dynamics, engineering applications and other challenges. Congreso de métodos numéricos en ingeniería 1–17
35. Baraldi D, Reccia E, Cecchi A (2018) In plane loaded masonry walls: DEM and FEM/DEM models. Critical Rev Meccanica 53:1613–1628. https://doi.org/10.1007/s11012-017-0704-3
36. Reccia E, Cazzani A, Cecchi A (2012) FEM-DEM modeling for out-of-plane loaded masonry panels: a limit analysis approach. Open Civil Eng J 6:231–238. https://doi.org/10.2174/1874149501206010231
37. Reccia E, Leonetti L, Trovalusci P, Cecchi A (2018) A multiscale/multidomain model for the failure analysis of masonry walls: a validation with a combined FEM/DEM approach. Int J Multiscale Comput Eng 16:325–343. https://doi.org/10.1615/IntJMultCompEng.2018026988
38. Liberatore D, Addessi D (2015) Strength domains and return algorithm for the lumped plasticity equivalent frame model of masonry structures. Eng Struct 91:167–181. https://doi.org/10.1016/j.engstruct.2015.02.030
39. Addessi D, Sacco E (2014) A kinematic enriched plane state formulation for the analysis of masonry panels. Euro J Mech, A/Solids 44:188–200. https://doi.org/10.1016/j.euromechsol.2013.10.013
40. Addessi D, Ciampi V (2007) A regularized force-based beam element with a damage–plastic section constitutive law. Int J Numer Methods Eng 70:610–629. https://doi.org/10.1002/nme.1911
41. Facchini L, Betti M (2017) Time-history analysis of slender masonry towers: a parametric study on the reliability of a simplified Bouc and Wen approach. Meccanica 52:3181–3196. https://doi.org/10.1007/s11012-017-0671-8
42. Facchini L, Betti M (2016) Simplified seismic analysis of disordered masonry towers. ASCE ASME J Risk Uncertain Eng Syst A Civ Eng 2:C4015010. https://doi.org/10.1061/AJRUA6.0000856
43. Schiavoni M, Giordano E, Roscini F, Clementi F (2023) Numerical assessment of interacting structural units on the seismic damage: a comparative analysis with different modeling approaches. Appl Sci (Switzerland). https://doi.org/10.3390/app13020972
44. Giordano E, Masciotta MG, Clementi F, Ghiassi B (2023) Numerical prediction of the mechanical behavior of TRM composites and TRM-strengthened masonry panels. Constr Build Mater. https://doi.org/10.1016/j.conbuildmat.2023.132376
45. Salachoris GP, Magagnini E, Clementi F (2021) Mechanical characterization of "Scaglia Rossa" stone masonry through experimental and numerical analyses. Constr Build Mater. https://doi.org/10.1016/j.conbuildmat.2021.124572
46. Schiavoni M, Giordano E, Roscini F, Clementi F (2023) Advanced numerical insights for an effective seismic assessment of historical masonry aggregates. Eng Struct. https://doi.org/10.1016/j.engstruct.2023.115997
47. Schiavoni M, Giordano E, Roscini F, Clementi F (2023) Numerical modeling of a majestic masonry structure: A comparison of advanced techniques. Eng Fail Anal. https://doi.org/10.1016/j.engfailanal.2023.107293
48. Itasca Consulting Group Inc. (2013) 3DEC- 3D Distinct element code, version 5.0, user's manual
49. Chetouane B, Dubois F, Vinches M, Bohatier C (2005) NSCD discrete element method for modelling masonry structures. Int J Numer Methods Eng 64:65–94. https://doi.org/10.1002/nme.1358
50. Dubois F, Acary V, Jean M (2018) The contact dynamics method: a nonsmooth story. Comptes Rendus Mécanique 346:247–262. https://doi.org/10.1016/j.crme.2017.12.009
51. Midas FEA (2020) Analysis and algorithm manual
52. NTC2018 (2018) New Italian technical norms on constructions. DM 17/01/2018 aggiornamento delle "Norme tecniche per le costruzioni".
53. Explicative Notes for NTC2018 (2019) Circolare. 2009. Circolare no 617 del 2 febbraio 2009. In Istruzioni per l'applicazione delle nuove norme tecniche per le costruzioni di cui al decreto ministeriale 14 gennaio 2008
54. Lubliner J, Oliver J, Oller S, Oñate E (1989) A plastic-damage model for concrete. Int J Solids Struct 25:299–326. https://doi.org/10.1016/0020-7683(89)90050-4
55. Chen S, Ferrante A, Clementi F, Bagi K (2021) DEM analysis of the effect of bond pattern on the load bearing capacity of barrel vaults under vertical loads. Int J Masonry Res Innov. https://doi.org/10.1504/IJMRI.2021.116234

56. Lee J, Fenves GL (1998) Plastic-damage model for cyclic loading of concrete structures. J Eng Mech 124:892–900. https://doi.org/10.1061/(ASCE)0733-9399(1998)124:8(892)
57. Rafiee A, Vinches M, Bohatier C (2008) Application of the NSCD method to analyse the dynamic behaviour of stone arched structures. Int J Solids Struct 45:6269–6283. https://doi.org/10.1016/j.ijsolstr.2008.07.034
58. Rafiee A, Vinches M (2013) Mechanical behaviour of a stone masonry bridge assessed using an implicit discrete element method. Eng Struct 48:739–749. https://doi.org/10.1016/j.engstruct.2012.11.035
59. Rafiee A, Vinches M, Bohatier C (2008) Modelling and analysis of the Nimes arena and the Arles aqueduct subjected to a seismic loading, using the non-smooth contact dynamics method. Eng Struct 30:3457–3467. https://doi.org/10.1016/j.engstruct.2008.05.018
60. Castellazzi G, D'Altri AM, de Miranda S et al (2018) Numerical insights on the seismic behavior of a nonisolated historical masonry tower. Bull Earthq Eng 16:933–961. https://doi.org/10.1007/s10518-017-0231-6
61. Valente M, Milani G (2018) Effects of geometrical features on the seismic response of historical masonry towers. J Earthquake Eng 22:2–34. https://doi.org/10.1080/13632469.2016.1277438
62. Ferrante A, Schiavoni M, Bianconi F et al (2021) Influence of stereotomy on discrete approaches applied to an ancient church in Muccia, Italy. J Eng Mech. https://doi.org/10.1061/(ASCE)EM.1943-7889.0002000